TNO innovation for life

Modeling and Mitigation of Wind Turbine Noise Other Amplitude Modulation

TNO Public › TNO 2025 R10988
6 July 2025

Energy & Materials Transition
www.tno.nl
+31 88 866 50 65
info@tno.nl

TNO 2025 R10988 – 6 July 2025

Modeling and Mitigation of Wind Turbine Noise Other Amplitude Modulation

Author(s)	K. Boorsma
Classification report	TNO Public
Number of pages	19 (excl. front and back cover)
Number of appendices	0
Sponsor	RvO
Project name	BEST
Project number	060.54912

Summary

Within the BEST project, 'Blade Extensions for Silent Turbines', which ran from April 2023 to April 2025, the first commercially attractive application of permeable blade extensions 'Muteskin' for the reduction of noise in onshore wind is developed. As a subgoal of the project, the benefit of MuteSkin (and permeable blade extensions in general) for (secondary) wind turbine acoustic phenomena such as low-frequency noise and amplitude modulation are being investigated, and other physical mitigation strategies are explored. Within the present work, a feasibility assessment of modeling other amplitude modulation has been carried out. An integral modeling technique has been employed, which showed that local stall in case of high wind shear can result in other amplitude modulation, depending on the noise increase due to separated flow. This also implies that removing the stalled flow from the blade, e.g. by pitching the blades, can be an effective strategy to mitigate the mentioned modulation. It is recommended to validate the findings from the simulations by means of dedicated experiments, to further progress and reduce uncertainty on this topic.

BEST has been co-financed with Topsector Energiesubsidie from the Dutch Ministry of Economic Affairs under grant number HER+22-02-03415120.

Contents

1 Introduction

The fluctuating character of wind turbine sound contributes significantly to its perceived annoyance [1]. In field observations often refer to a 'rhythmic' character where the frequency corresponds to the rotational frequency of the rotor. This phenomenon is often labelled as Amplitude Modulation (AM), where two different types of AM can be defined. 'Normal' Amplitude Modulation (NAM) is apparent in sideways direction in proximity to the turbine (nearfield) and is caused by the combination of the directivity pattern of the dominant trailing edge noise source together with the effect of convective amplification due to the rotating character of the noise source [2]. In literature this type of AM is often referred to as swish. 'Other' Amplitude Modulation (OAM) is less well understood, but has been reported to be audible in the farfield (kilometers distance) and most prominently in the upwind and downwind direction [1]. Apart from field observations, the attempts to model OAM are scarce. It has been hypothesized that OAM is caused by local flow separation at the outboard part of the blades, e.g. in case of a blade pointing upward in a pronounced vertical wind shear [3, 4]. Integral modelling of time varying source strength on a rotating blade together with propagation effects is not trivial and requires model fidelity choices to manage the computational effort. As a consequence there have been also very few efforts to reduce OAM. The current study contributes to the further understanding of the possible cause of OAM by using a systematic integral modelling approach, which can pave the way to the evaluation of possible mitigation techniques.

2 Methodology

To model the integral effects of varying blade noise source levels together with propagation effects, the Silant tool [5] has been used. Two different strategies are pursued to model the varying noise source strength due to flow separation in case of a vertical shear. Further details are give in section 2.1 and the following sections of this chapter.

2.1 Reference noise model

Silant [5] originated in 1996 from a Dutch consortium consisting of Stork Product Engineering BV, the Netherlands Organisation for Applied Scientific Research (TNO) and the Dutch Aerospace Laboratory (NLR). The model was designed to calculate noise emission of wind turbines, based on the sources that are considered most important: trailing edge noise (including separation-stall noise) and inflow noise. After the Energy Research Center of the Netherlands (ECN) became the manager of the tool, several improvements have been made, partly in cooperation with NLR. The improvements include the addition of models for prediction of tip noise and propagation effects. From 2018 ECN has become part of TNO, which has returned the software tool to one of its original developers.

The approach of Silant to calculate the noise levels is to divide the rotor blades into a number of equidistant segments, usually in the order of 10 to 20 per blade. For each element, the trailing edge and inflow noise source are calculated according to the model of Brooks Pope and Marcolini (BPM) [6] and the model of Amiet [7] and Lowson [8] respectively. For the tip element, the contribution of tip noise is added [6]. To determine the total emission, the element contributions are acoustically summed, assuming the sources to be incoherent. Optionally the sound pressure levels are calculated for specified receiver positions, located in a polar grid around the turbine.

The propagation effects are calculated separately for each element-receiver combination and source. Tip noise is treated as trailing edge noise for this purpose. The actual turbine geometry dependent parameters (i.e. location, orientation and velocity of each blade element) are determined from specified radial location, hub height, pitch-, tilt- and cone angle, azimuth position and rotational speed. For the default model, the acoustic source strength is assumed constant over a rotor revolution. Equation 2.1 shows how the contributions are incorporated to obtain the immission of an element-receiver combination.

$$SPL = PWL + L_{DI} + L_{CA} + L_{spread} + L_{att} + L_{meteo} \quad , \tag{2.1}$$

with

SPL	[dB]	Sound Pressure Level
PWL	[dB]	Power Watt Level
L_{DI}	[dB]	directivity
L_{CA}	[dB]	convective amplification
L_{spread}	[dB]	geometrical spreading
L_{att}	[dB]	atmospheric attenuation
L_{meteo}	[dB]	refraction and ground effect

In addition to the above mentioned effects that mainly modify the overall noise level, a

redistribution of the sound over the frequency domain is performed according to the Doppler effect. After the propagation effects have been incorporated, A-weighting of the sound pressure levels can be applied. It is beyond the scope of this report to discuss the technical nature of the different contributions of the propagation model. In the current project, the refraction and ground effect are not considered. For more details, the reader is referred to the dedicated publication about the tool [5].

The Silant model requires input of the quasi steady rotor aerodynamic state. In practice, the distribution of angle of attack and effective velocity as a function of blade span are pre-calculated using a code like BladeMode [9] that resolves the rotor aerodynamics. However the periodic noise increase due to flow separation or stall requires the input of a time varying noise source with rotor azimuth angle. Two different approaches are adopted to mimic this effect, which are explained below.

2.2 Imposing impulsive noise variation

Instead of using a physical model to predict the noise source change due to local separation or stall, one can also impose a fixed noise increase for a certain radial extent on the blade, depending on the azimuth angle. With this 'quick and dirty' approach, it can be verified how such a temporary noise increase would propagate into the farfield. As the directivity pattern of separation stall noise resembles a dipole shape, the noise addition is programmed incremental to the inflow noise source. The specifications of the noise increase are summarized in Table 2.1. See also Figure 2.1 for a visualization of the noise distribution over the rotor plane for a

Table 2.1: Specifications of the imposed impulsive noise variation.

Parameter	Unit	Value	Comment
Level increase	[dB]	10	Constant over the frequency range
Noise source type	[-]	inflow	
Radial extent	[%R]	>88	
Azimuthal extent	[deg]	[-15,15]	Zero degree corresponds to blade pointing up

5MW rotor as defined in section 2.3.1.

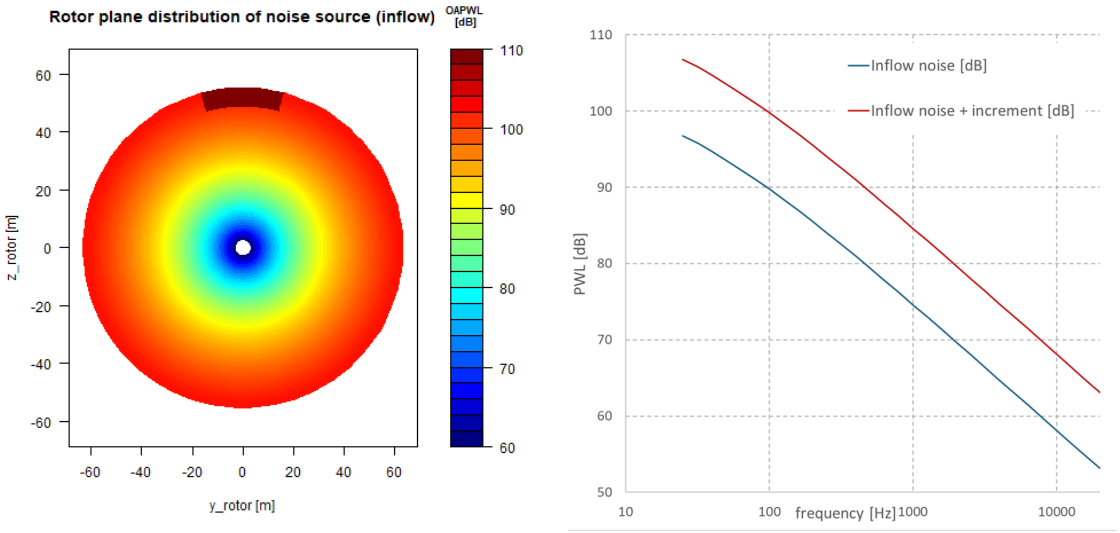

(a) Inflow noise source distribution over the rotor plane

(b) Inflow noise source spectra at the tip

Figure 2.1: Definition of impulsive noise increment to inflow noise source for a 5MW rotor

2.3 Physical modeling of separation-stall noise

The BPM model [6] contains a switch between turbulent boundary layer trailing edge noise and separation-stall noise. A user specified angle of attack can be used to switch between the two noise sources dependent on the operational conditions. As such we can, by varying angle of attack and effective inflow speed, distinguish between noise source spectra for design and separated flow conditions. For the current research a special version of Silant is compiled which allows the calculation of blade azimuth dependent noise sources by feeding angle of attack and effective velocity variations with azimuth angle and radial position. To estimate these input parameter variations, we can perform aero-elastic simulations under different sheared inflow conditions. These are discussed in the next section.

2.3.1 Aero-elastic simulation

The ART 5MW turbine [10], which is based on the NREL 5MW turbine [11] featuring a re-designed rotor, is subject of investigation. See also table 2.2 for the main specifications of this turbine. For the current study, the turbine is modelled rigid. The operational condition

Table 2.2: Summary of main specifications of the ART 5MW turbine.

Parameter	Unit	Value
Rotor diameter	[m]	128.4
Hub height	[m]	90
Rated power	[MW]	5
Rated rotor speed	[rpm]	12.393
Rated tip speed	[m/s]	83.3
Control	[-]	Variable speed, collective pitch
Rotor orientation	[-]	upwind
Nuber of blades	[-]	3
Tilt angle	[deg]	5
Cone angle	[deg]	-2.5

under investigation is in the so-called knee of the power curve, where the noise source levels peak at a wind speed of 10.5 m/s around rated rotor speed and zero pitch angle.

A vertical wind shear is commonly defined using a shear exponent α according to equation 2.2.

$$U_i = U_{hub}(z_i/z_{hub})^{\alpha} \tag{2.2}$$

with

z_i	[m]	height of interest above ground level
U_i	[m/s]	wind velocity at height z_i
U_{hub}	[m/s]	hub height wind velocity
z_{hub}	[m]	hub height above ground level
α	[-]	shear exponent

For two different shear exponents, rotor aerodynamic simulations are performed using the TNO Aero Module code [12], which contains both a Blade Element Momentum (BEM) and a Free Vortex Wake (FVW) method. In line with previous research concerning the accuracy of sheared inflow simulations [13], FVW simulations are performed to minimize the uncertainty in the resulting angle of attack and effective velocity distributions. The shear profiles under consideration are chosen to cover the operational regime, where an exponent of $\alpha = 0.25$ corresponds to daytime conditions and $\alpha = 0.5$ corresponds to a very stable atmosphere at night. The resulting shear profiles are illustrated in Figure 2.2.

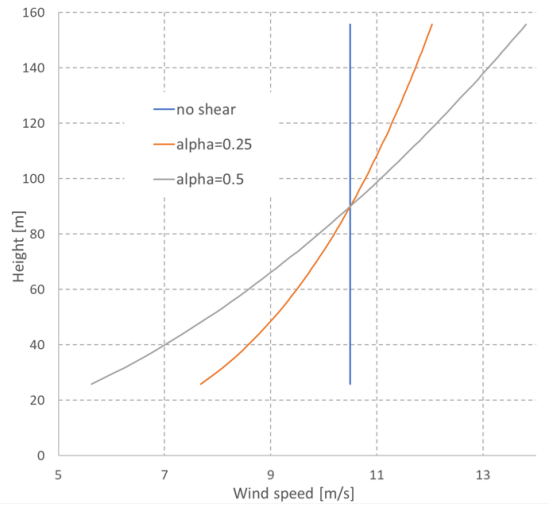

Figure 2.2: Illustration of vertical shear profiles over rotor plane height

The predicted angle of attack and effective velocity variations corresponding to these shear profiles are illustrated in Figures 2.3 and 2.4. It can be shown that the angle of attack roughly follows a harmonic variation owing to the variation of axial wind speed around the revolution. The effective wind speed variation is relatively small and more dominated by the tangential velocity component which in this case is driven by the advancing and retreating blade effect caused by the tilt angle of the rotor (peaking around 90° rotor azimuth). It is noted that a yaw angle misalignment induces variations that peak at 0° or 180° which could influence the amount of flow separation. For some manufacturers it is common practice to purposely misalign the turbine to reduce the periodic load variation due to shear, by reducing the angle of attack variation. So this is expected to reduce the amount of potential flow separation.

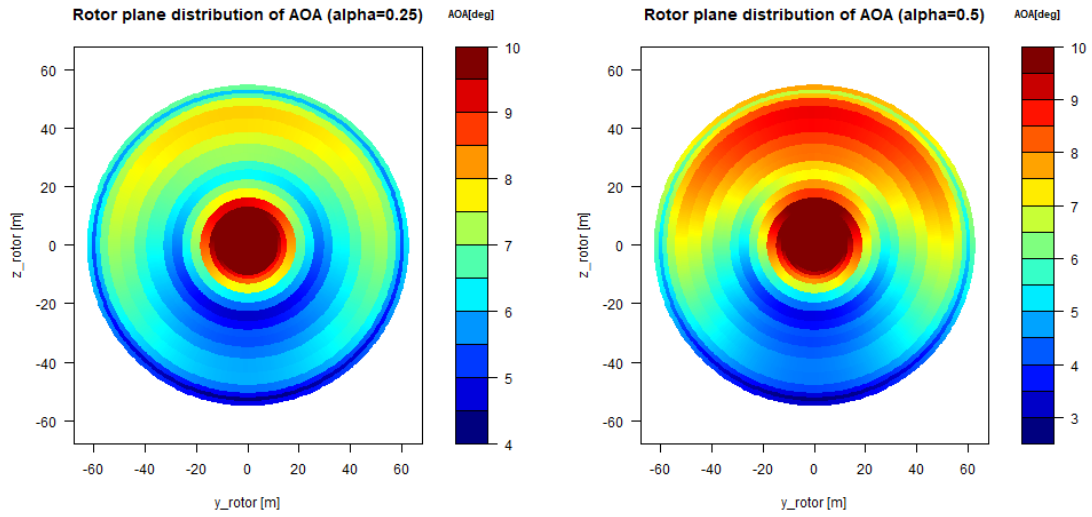

(a) $\alpha = 0.25$ (b) $\alpha = 0.50$

Figure 2.3: Illustration of predicted angle of attack variation over the rotorplane.

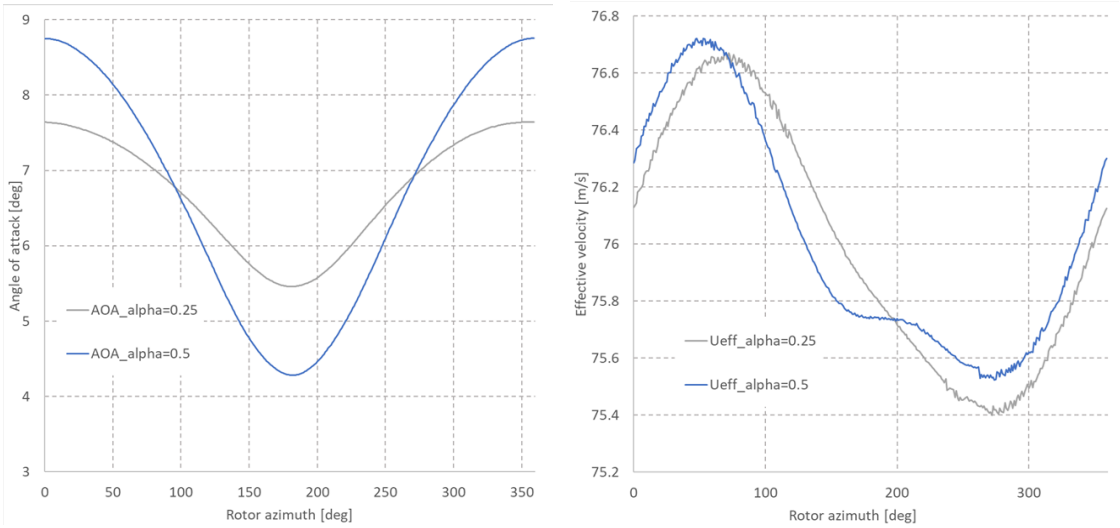

(a) Angle of attack (b) Effective velocity

Figure 2.4: Illustration of predicted aerodynamic performance variation as function of rotor azimuth angle at 90%span

Figure 2.5 then shows the lift and drag curve for the NACA63418 profile which has been used in the outboard part of the blades for this turbine. Acknowledging the stall angle of attack for this airfoil around 14 degrees, this indicates that even for the heavy vertical shear with an exponent of 0.5, the outboard section would not enter into stall for the blade pointing upward. Considering that a safe stall margin between design and stall angle of attack of around 5 degrees is commonplace in blade design, it is quite a challenge to stall the outboard part of wind turbine blades during normal operation. A consideration that can be added here, is the fact that rough or eroded blade surfaces can negatively affect airfoil stall performance.

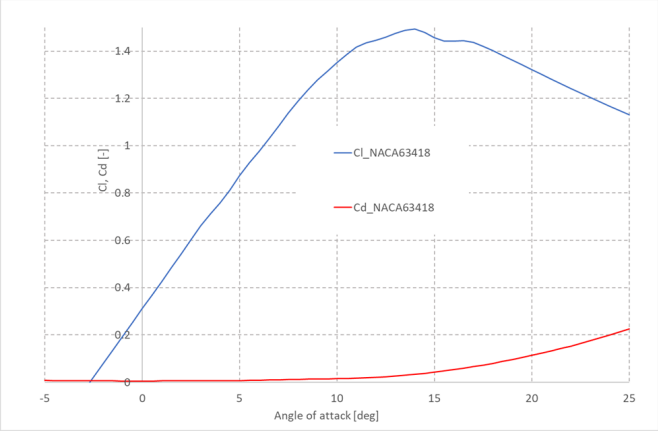

Figure 2.5: Lift and drag polars for the NACA63418 profile.

2.3.2 Resulting noise source characteristics

The predicted angle of attack and effective velocity variations from the shear simulations have been inputted to the Silant code to evaluate the noise source variation across the rotorplane. The left part of Figure 2.6 then shows the resulting noise distribution in case of the heavy shear profile, clearly indicating an increase in noise for the upper part of the rotorplane as expected.

However the changes in noise source level are quite smooth, mainly owing to the harmonic angle of attack variation. If we lower the stall angle of attack α_{stall} to 8.5 ° (visualized in the right par of Figure 2.6), we can identify a slight elevation of source levels up to 2 dB, which has a more discontinuous character roughly 30 ° in rotor azimuth separated from the upward blade position on both sides. This increase follows the separation-stall noise toggle intrinsic to the BPM model [6], that is activated once the angle of attack exceeds the specified stall angle. This noise increase is considerably lower than the 10dB increase used in previous work [3]. Here it is stated that separation stall noise prediction is associated with a considerable uncertainty, owing to the lack of validation material and the impact of differences in stalling behaviour (e.g. abrupt leading edge stall or gradual trailing edge stall) between airfoils. However the current BPM implementation is believed to be the most accurate up to date, as it has been validated also in separated flow conditions against the New Mexico database [14], where the NACA64418 profile has been used for the outboard sections. It is recommended to perform further validation of separation-stall noise modeling at airfoil level, e.g. using the measurements from [4], which did show a more substantial noise increase for stalled conditions, predominantly in the lower frequency range.

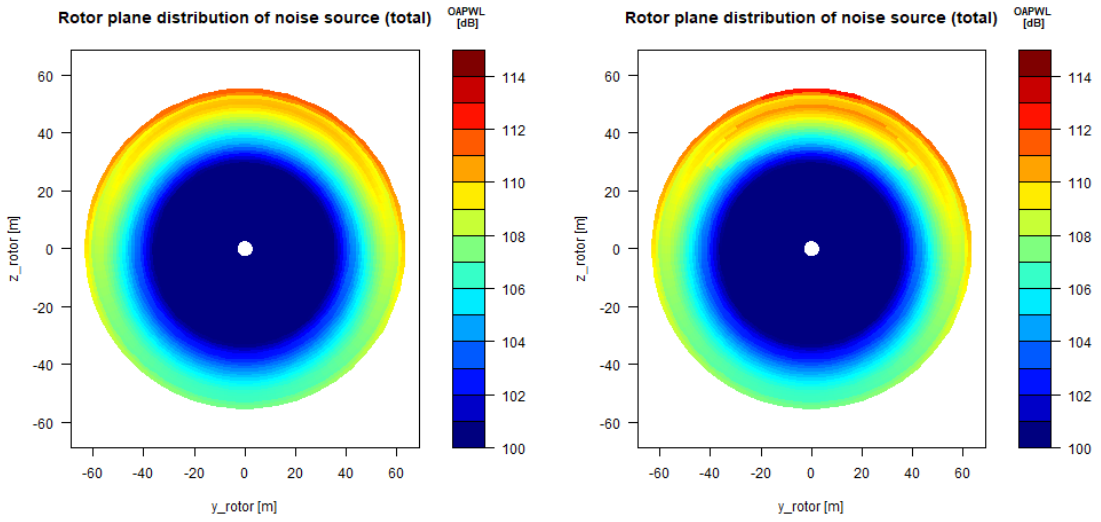

(a) $\alpha_{stall} = 14\,°$ (b) $\alpha_{stall} = 8.5\,°$

Figure 2.6: Illustration of predicted noise source variation over the rotorplane for a shear exponent of $\alpha = 0.50$, employing two different stall angles of attack. Noise levels are non-weighted.

The previously illustrated noise source plots did not include the A-weighting that is commonly used to correct for the perception of the human ear. Figure 2.7 (left plot) shows that including this A-weighting leads to a more prominent noise increase in case of flow separation. The right hand side plot of Figure 2.7 explains the cause for this difference by analysing the frequency spectrum. Although the non-weighted noise peak is not really affected by the separation-stall noise for the blade pointing upwards, the hump is broadened towards higher frequencies. Since the A-weighting progressively decreases the lower frequency noise levels, these higher frequencies shape the A-weighted peak levels, hence giving rise to elevated overall noise levels.

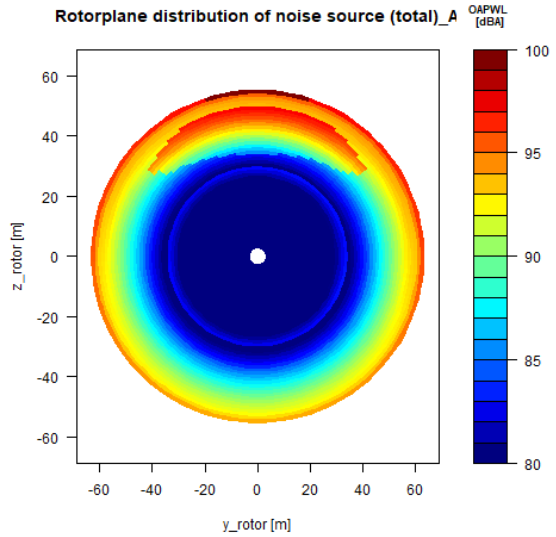

(a) A-weighted noise source variation over the rotorplane, $\alpha_{stall} = 8.5\,^{\circ}$

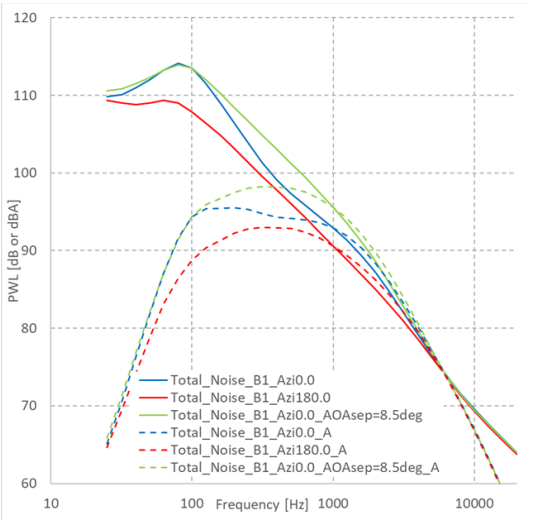

(b) Difference between A-weighted (dashed) and non-weighted (solid) 1/3-Octave band blade noise source spectra for different azimuth angles

Figure 2.7: Impact of A-weighting on the predicted noise source levels for a shear exponent of $\alpha = 0.50$.

3 Results

Finally it is evaluated how the noise source variation propagates. Therefore a polar grid in defined at ground level as illustrated in Figure 3.1. The radial discretization is as illustrated. The distance between the specified maximum radius (r_max = 1000 m) and 0.1 times the rotor radius is subdivided by the number of given radial locations (n_r=10). The discretization in polar direction is also illustrated and is defined by the number of polar locations (n_phi = 36).

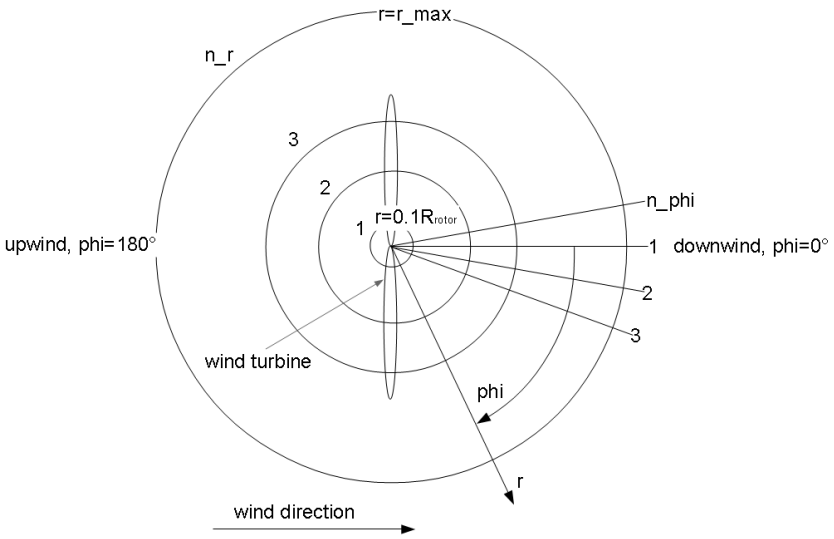

Figure 3.1: Illustration of polar grid: Top view of turbine lay-out

The time step of the simulations is defined in terms of a step in rotor azimuth angle, which is specified to 3.33 ° in this case. Refraction and ground effects are omitted in the propagation calculation.

Figure 3.2 shows the noise footprint for a reference case with a constant noise source. From literature [2, 5] it is known that trailing edge noise is the dominant source for conventional wind turbines and its directivity pattern together with convective amplification effects result in the highest noise levels in up- and downwind direction. However the temporal variation of noise or swish caused by the same effects is most dominant in the sideways directions.

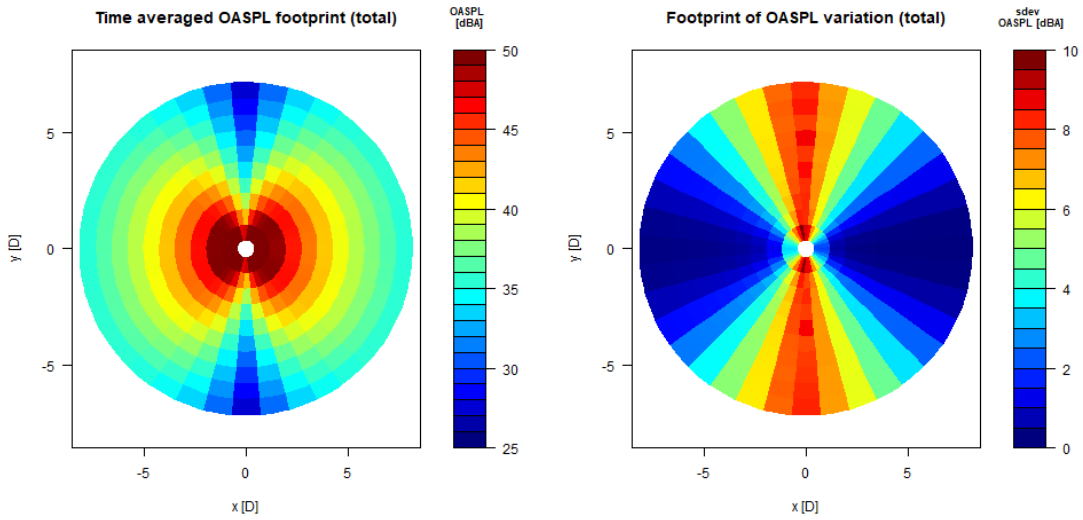

(a) Time averaged values

(b) Variation amplitude (max - min)

Figure 3.2: Illustration of A-weighted OASPL footprints at ground level for the reference case. Distances are expressed in turbine diameters D, x and y denote axial and sideway direction respectively.

3.1 Imposing impulsive noise variation

As mentioned above and visualized in Figure 2.1, the impulsive noise variation is considered incremental to inflow noise. An illustration of the predicted temporal variation at several polar locations is given in Figure 3.3. It is clear that the step in noise level persists at several polar angles, compared to a relatively flat line for the reference case.

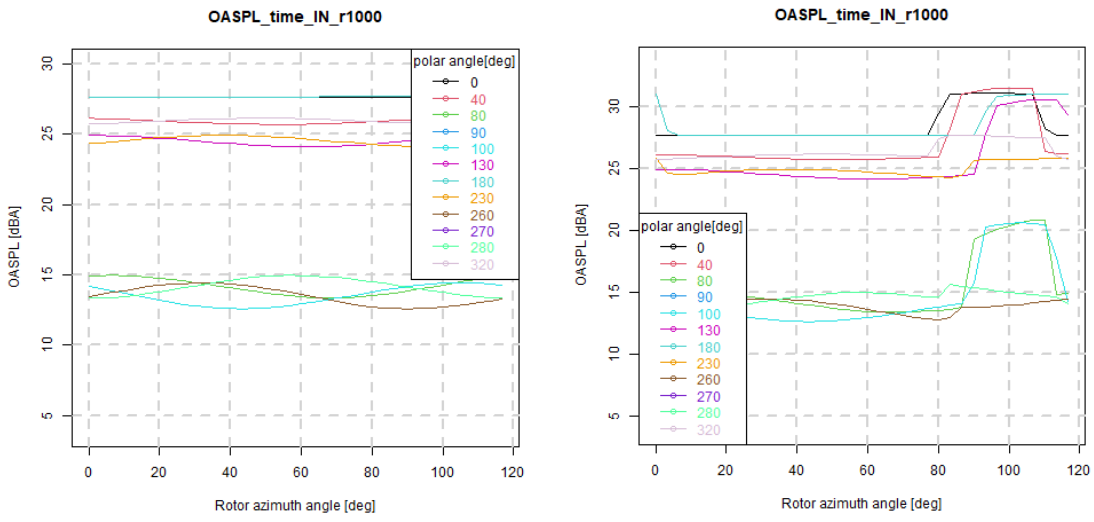

(a) Reference case

(b) Impulsive noise variation

Figure 3.3: Impact of impulsive noise on temporal noise variation at 1000m from the turbine for various polar angles as function of rotor azimuth angle.

To facilitate the interpretation, the amplitude (max - min) has been plotted as function of

polar angle for various distances in Figure 3.4. It is clear that the largest amplitudes occur in sideways direction towards the blade movement direction for the upward pointing blade. The differences in variation between the polar angles were found to be caused by a combination of convective amplification, noise directivity and Doppler-induced weighting effects. It also becomes clear that significant variation amplitudes of almost 4dB perist in the upwind and downwind direction. This observation points towards confirmation of the hypothesis that a sudden noise increase with a dipole character occuring for an upward pointing blade gives rises to noise fluctuations that propagate in the audible part of the farfield noise (upwind/downwind direction).

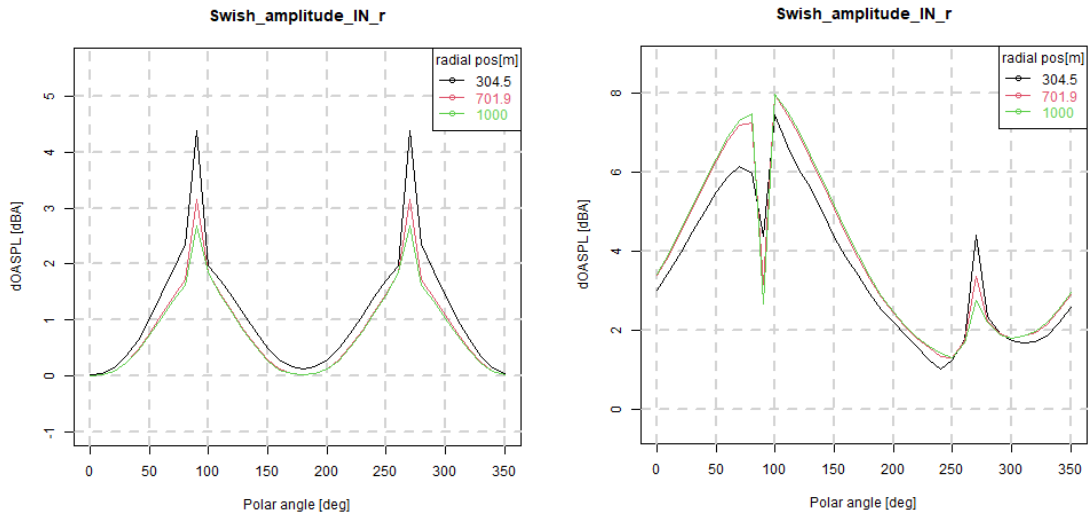

(a) Reference case

(b) Impulsive noise variation

Figure 3.4: Impact of impulsive noise on swish amplitudes at various distances from the turbine as function of polar angle.

3.2 Physical modeling of separation-stall noise

The resulting noise source variation in case of a large vertical wind shear with an exponent of 0.4 was calculated in section 2.3.2. Here it was shown that the stall margin was not exceeded for the outboard part of the blade. Figure 3.5 shows harmonic noise variations for most polar angles, expect for the upwind and downwind directions (0 ° and 180 °) . The swish amplitudes are larger again in the direction of rotation for the upward blade position (polar angles smaller than 180 °), mainly due to the convective amplification. The temporal variation in sideway directions shows wiggles, probably due to the discontinous character of the directivity function of training edge noise in this direction. It is also noted from the temporal variations that the absolute noise levels at polar angles of 40 °, 130 ° and to a lesser extent at 230 ° and 320 ° are similar to the upwind and downwind levels, and still feature a considerable swish amplitude up to 4dBA. However, as can be concluded from the results of the reference simulation in Figure 3.2, this is also the case if shear is not present.

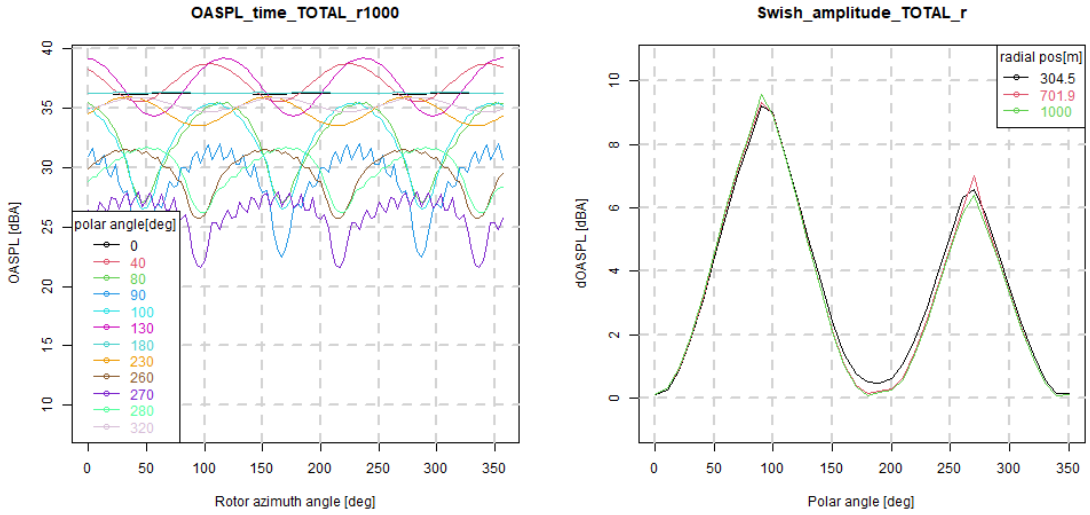

(a) Temporal noise variation at 1000m from the turbine for various polar angles as function of rotor azimuth angle

(b) Swish amplitudes at various distances from the turbine as function of polar angle

Figure 3.5: Perceived noise levels for the simulation with vertical wind shear (exponent of 0.4).

Subsequently, the effect of stall on perceived noise levels was examined in Figure 3.6 by lowering the specified stall angle of attack. It can be observed that the swish amplitudes in upwind and downwind direction are elevated from zero by approximately 1 dBA. Hence, although the noise increase due to stall impacts the farfield fluctuations, it is too small to significantly impact noise perception for this case. However if separation-stall noise elevation levels would increase significantly, the noise fluctuations are expected to propagate in the farfield resulting in considerable OAM. This also implies that removing the stalled flow from the blade, e.g. by pitching the blades, can be an effective strategy to mitigate the mentioned OAM phenomenon. Considering the uncertainty in predicting separation-stall noise levels and propagation effects, this is something to have a closer look at including validation in wind tunnel and field environment.

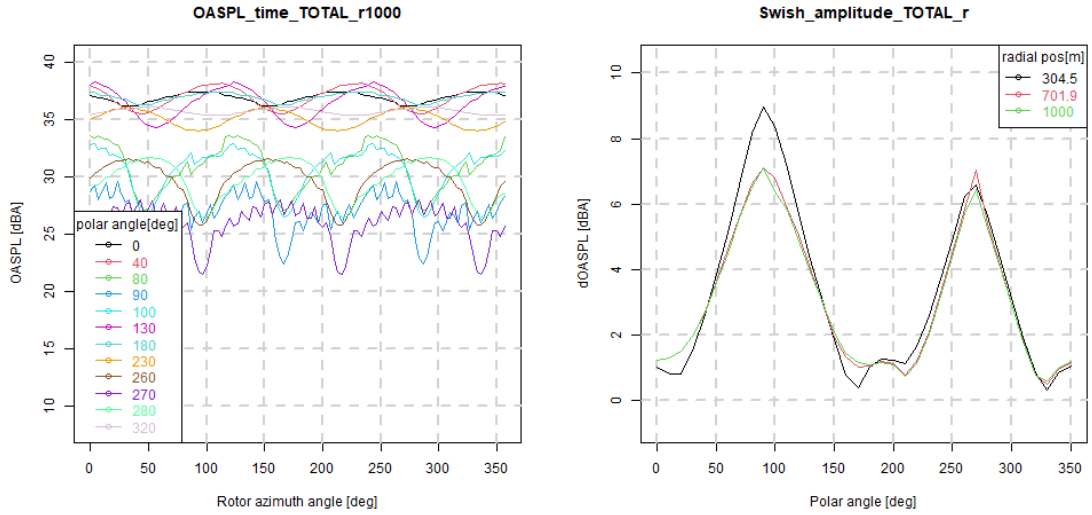

(a) Temporal noise variation at 1000m from the turbine for various polar angles as function of rotor azimuth angle

(b) Swish amplitudes at various distances from the turbine as function of polar angle

Figure 3.6: Perceived noise levels for the simulation with vertical wind shear (exponent of 0.4) and a modified stall angle of attack ($\alpha_{stall} = 8.5\,°$)

4 Conclusions and recommendations

A further understanding of the possible causes of Other Amplitude Modulation (OAM) of wind turbine noise has been obtained. Hereto a systematic integral modelling approach has been developed and applied for a joint evaluation of time varying noise source strength on a rotating blade together with propagation effects in a computationally efficient manner. It has been found that, in agreement with previous research, a sudden local noise source increase with a dipole directivity for upward blade positions can significantly contribute to OAM in the farfield.

Subsequently it was examined whether local stall in case of high wind shear could cause a source contribution with the described signature. Here it was found that although the noise increase due to stall impacts the farfield fluctuations, it is too small to significantly impact noise perception for this case. However if separation-stall noise elevation levels would increase significantly, the noise fluctuations are expected to propagate in the farfield resulting in considerable OAM. This also implies that removing the stalled flow from the blade, e.g. by pitching the blades, can be an effective strategy to mitigate the mentioned OAM phenomenon.

As a next step it is recommended to perform more parameter variations, to shed more light on the required conditions for the occurrence and mitigation of OAM. Furthermore, dedicated field and wind tunnel experiments are required to validate the findings from the simulations.

References

[1] G.P. van den Berg. “The Relevance of AM Mitigation.” In: *10th Convention of the European Acoustics Association*. Turin, Italy, Sept. 2023.

[2] S. Oerlemans and J.G. Schepers. “Prediction of wind turbine noise and validation against experiment.” In: *Internation Journal of Aeroacoustics* 8.6 (2009).

[3] S. Oerlemans. “Effect of wind shear on amplitude modulation of wind turbine noise.” In: *Aeroacoustics* 14.5 (2015), pp. 715–728.

[4] A. Fischer et al. “Analyses of the mechanisms of amplitude modulation of aero-acoustic wind turbine sound.” In: *Proceedings of European Wind Energy Association Conference and Exhibition 2014*. Barcelona, Spain, Mar. 2014.

[5] K. Boorsma and J.G. Schepers. “Enhanced wind turbine noise prediction tool SILANT.” In: *Conference proceedings of fourth International Meeting on Wind Turbine Noise*. Rome, Italy, Apr. 2011.

[6] T.F. Brooks, D.S. Pope, and M.A. Marcolini. *Airfoil self noise and prediction*. Tech. rep. Reference publication 1218. NASA, 1989.

[7] R.K. Amiet. “Acoustic Radiation From an Airfoil in a Turbulent Stream.” In: *Journal of Sound and Vibration* 41.4 (Apr. 1975), pp. 407–420.

[8] M.V. Lowson. *Assessment and Prediction of Wind Turbine Noise*. Tech. rep. Flow Solutions Report 92/19. ETSU W/13/00284/REP, Dec. 1992, pp. 1–59.

[9] C. Lindenburg. *Bladmode, Program for Rotor Blade Mode Analysis*. Tech. rep. ECN-C–02-050-r2. ECN, 2002.

[10] K. Boorsma et al. *Smart Rotor Design, Technology Assessment*. Tech. rep. ECN-X–11-154. ECN, Dec. 2011.

[11] J. Jonkman et al. *Definition of a 5-MW Reference Wind Turbine for Offshore System Development*. Tech. rep. NREL/TP-500-38060. NREL, Feb. 2009.

[12] K. Boorsma, F. Grasso, and J.G. Holierhoek. *Enhanced approach for simulation of rotor aerodynamic loads*. Tech. rep. ECN-M–12-003. ECN, presented at EWEA Offshore 2011, Amsterdam, 29 November 2011 - 1 December 2011.

[13] K. Boorsma et al. “Challenges in Rotor Aerodynamic Modeling for Non-Uniform Inflow Conditions.” In: *Journal of Physics: Conference Series* 2767.2 (June 2024), p. 022006. DOI: 10.1088/1742-6596/2767/2/022006. URL: https://dx.doi.org/10.1088/1742-6596/2767/2/022006.

[14] K. Boorsma and J.G. Schepers. “Wind turbine noise measurements in controlled conditions.” In: *International Journal of Aero-acoustics* 16.7-8 (2017), pp. 649–665.

Energy & Materials Transition

Westerduinweg 3
1755 LE Petten
www.tno.nl

TNO innovation for life